Supplement to: The generic nature of the tropospheric response to sudden stratospheric warmings

Ian White*

The Hebrew University of Jerusalem, Institute of Earth Sciences, Edmond J. Safra Campus, Givat Ram, Jerusalem, Israel

Chaim I. Garfinkel

The Hebrew University of Jerusalem, Institute of Earth Sciences, Edmond J. Safra Campus, Givat Ram, Jerusalem, Israel

Edwin P. Gerber

Courant Institute of Mathematical Sciences, New York University, New York, USA

Martin Jucker

Climate Change Research Centre, University of New South Wales, Sydney, Australia

Peter Hitchcock

Department of Earth and Atmospheric Sciences, Cornell University, New York, USA

Jian Rao

The Hebrew University of Jerusalem, Institute of Earth Sciences, Edmond J. Safra Campus, Givat Ram, Jerusalem, Israel

Corresponding author address: Ian White, The Hebrew University of Jerusalem, Institute of Earth Sciences, Edmond J. Safra Campus, Givat Ram, Jerusalem, Israel.
E-mail: ian.white@mail.huji.ac.il

ABSTRACT

21

1. Model

a. Model Setup

As mentioned in the main manuscript, this study uses the Model of an Idealised Moist Atmosphere (MiMA Jucker and Gerber 2017). Our model setup for the 50-year free-running control integration (CTRL) is is essentially the same as that recently developed by Garfinkel et al. (2019, hereafter G19), but with some slight differences in the albedo profile and prescribed q-fluxes (see sections 3a and 3b, respectively, in G19 for details and notation). In terms of the q-flux profile, we prescribe q-fluxes in the vicinity of the Gulf Stream and Kuroshio Current which are taken here to have maximal values of $Q_{\mathrm{Gulf}} = 100\mathrm{W\ m}^{-2}$ and $Q_{\mathrm{Kuroshio}} = 30\mathrm{W\ m}^{-2}$, respectively. These are larger than the $Q_{\mathrm{Gulf}} = 60\mathrm{W\ m}^{-2}$ and $Q_{\mathrm{Kuroshio}} = 25\mathrm{W\ m}^{-2}$ prescribed in G19. G19 further incorporated heat transport over the North Sea to approximate observed q-fluxes, but these are omitted here.

In terms of albedo, we use a latitudinal step profile as compared to a smoother *tanh* profile used in G19. In particular, a baseline albedo of 0.26 (to approximate the shortwave effect of clouds) in our study is increased south of 70°S to a value of 0.65 to approximate the higher albedo over Antarctica. In G19 these values are 0.27 and 0.75 with a smooth transition between the two. G19 further include a term to smoothly increase the albedo over the Arctic, but this is omitted here. Note that these differences in q-fluxes and albedo do not affect our results quantitatively.

b. Control Run Climatology

In figure 1, we present the December-February (DJF) climatologies of the zonal-mean zonal wind $\overline{u}$, zonal-mean temperature $\overline{T}$ and the quasi-geostrophic refractive index n^2 for the 50-year control run (CTRL). Note that n^2 is calculated similarly to in the main article, except that $\overline{u}$ and $\overline{T}$ are first averaged over DJF before calculating $\overline{q}_\varphi$. It is clear that the polar vortex in CTRL is too strong and cold compared to that observed (e.g., Andrews et al. 1987). Such model biases in the background state can be problematic in identifying SSWs using absolute thresholds such as the reversal of $\overline{u}$ at 60°N, 10 hPa as it can underestimate the number of SSWs (e.g., **?**).

The refractive index n^2 (b; calculated for a stationary planetary wave with $k = 1$ and $c = 0$) is very similar to that found in observations (e.g., Andrews et al. 1987) with a minimum near 40°N in the lower stratosphere and very large values close to the zero-wind line in the subtropics. Hence, Rossby waves (as identified using the Eliassen-Palm flux; climatology not shown) propagate upward and equatorward, avoiding the n^2 minimum in the midlatitude lower stratosphere.

2. Refractive Index Evolution

This figure should be compared with the n^2 and $\overline{q}_\varphi$ anomalies shown in figure 9 in the main manuscript.

3. Wave-flux Diagnostics

We here provide further diagnostics of the EP fluxes in order to emphasise the linearity of the tropospheric and stratospheric response to the imposed forcing, as well as an analysis of the

Eulerian mean momentum budget.

To understand how the wave anomalies change for different thermal forcing, figure 3a shows timeseries of synoptic-wave $F^{(\varphi)}$ area-averaged over 45-55N and vertically integrated over 500-200 hPa, for each PTRB heating run and for CTRL. These latitude and pressure-level ranges were chosen so as to approximately capture the region of anomalous tropospheric synoptic-wave anomalies shown in figures 6-7 in the main manuscript. In CTRL, $F^{(\varphi)} > 0$ is found at most lags, in agreement with figure 6 in the main text, although it is not always significantly different from the climatology. After lag 21 (marked by a vertical dashed line), CTRL and PTRB are generally similar with $F^{(\varphi)} > 0$. In general, PTRB runs with stronger thermal forcing yield larger-magnitude $F^{(\varphi)}$ anomalies. Nevertheless, there is some overlap between different experiments due to internal tropospheric variability. Note that the $F^{(\varphi)} < 0$ at lags 10-20 in PTRB, is related to the EP-flux fountain present in figure 7b in the main manuscript which forms as a result of the induced tropospheric westerlies shown in figures 2b-d.

Figure 3b shows the planetary-wave $F^{(z)}$ area-averaged over 50-80N and vertically integrated over 150-5 hPa to highlight the planetary-wave suppression following the SSWs. In CTRL, the preceding anomalous upward wave activity is clearly evident. After the onset, there is a suppression of planetary waves for all PTRB experiments, although it is insignificant for the 5-K PTRB. The suppression is of similar magnitude to the CTRL $F^{(z)}$ at lags $>$10, after which the PTRB and CTRL anomalies evolve very similarly. The PTRB ensemble means are clearly separated, with stronger thermal forcing yielding stronger planetary-wave suppression after the onset date. The suppression lasts for $\sim 80-90$ days in all experiments.

To examine the momentum balance in the tropospheric jet shift region, figure 3c shows the Eulerian mean momentum budget:

$$\frac{\partial \overline{u}}{\partial t} = f\overline{v} - \frac{1}{a\cos^2\varphi}(\overline{u'v'}\cos^2\varphi)_\varphi - \overbrace{\left[\frac{\overline{v}}{a\cos\varphi}(\overline{u}\cos\varphi)_\varphi + \frac{1}{\rho_0}(\rho_0\overline{w'u'})_z + \overline{w}\frac{\partial \overline{u}}{\partial z}\right]}^{\text{ageostrophic terms}} + \overline{X} \qquad (1)$$

(e.g., Andrews et al. 1987) averaged over 50-65N and vertically-integrated over 700-200 hPa (chosen to coincide with the polar $\overline{u} < 0$ anomalies). It is clear that the dominant balance is between the eddy momentum flux convergence ($-(a\cos^2\varphi)^{-1}(\overline{u'v'}\cos^2\varphi)_\varphi$) and the coriolis torque acting on the mean meridional circulation ($f\overline{v}$) with the ageostrophic terms being small. $\partial\overline{u}/\partial t$ is well approximated by the sum of the other terms. In particular, $\partial\overline{u}/\partial t$ is negative for the first ~35 days after which it oscillates around zero (but insignificant). Overall, this indicates that there is a divergence of momentum from high latitudes (i.e., a convergence of the EP flux) which is balanced by a poleward meridional circulation (see figure 10 in main text) in agreement with Simpson et al. (2009).

4. The Residual Circulation

a. Residual Circulation Decomposition

Figures 4- 5 show the same as in figure 10 in the main manuscript, except for the contribution of the $\Psi_{\overline{v}}$ and $\Psi_{\overline{v'\theta'}}$ to the full residual mean meridional circulation Ψ^*.

b. Stratospheric NAM Variability

In figure 10 in the main article, the tropospheric response of the residual mean meridional circulation Ψ^* to a SSW was a tripole with $\Psi^* > 0$ at midlatitudes, flanked at low and high latitudes by $\Psi^* < 0$. We here show that this feature is actually the tropospheric response to general stratospheric NAM variability. In figure 6, Ψ^* (shading) and $\overline{u}$ (contours) are regressed (as a function of latitude and pressure) onto the NAM index in both the troposphere (a; 500 hPa) and stratosphere (b; 10 hPa). Both are then scaled by the magnitude of the November-April NAM index at that level, to ensure the same units as in figures 2 and 10 in the main article.

Regressed onto the tropospheric NAM (a), $\overline{u}$ shows a dipole which approximately straddles the climatological jet maximum, with $\overline{u} < 0$ ($\overline{u} > 0$) on the poleward (equatorward) flank of the jet. This dipole extends into the stratosphere, peaking near 70N, 10hPa. The Ψ^* response is a dipole of opposite-sign to the $\overline{u}$ dipole in the troposphere and likely represents a change in the width of the Ferrel cell.

Regressed instead onto the 10-hPa NAM (b), the tropospheric response to a negative stratospheric NAM is a $\overline{u}$ dipole which weakly penetrates down to 700 hPa. In Ψ^*, the response is $\Psi^* > 0$ in the stratosphere (indicating a strengthened Brewer-Dobson circulation as observed in the onset of a SSW), and a tropospheric tripole with $\Psi^* > 0$ at midlattidues, flanked at low and high latitudes by $\Psi^* < 0$. The tropospheric response is very similar to that found in figure 10 in the main article following a SSW. It represents changes in the width of the Polar, Ferrel and Hadley cells (e.g., Martineau et al. 2018). The relatively weak penetration of $\overline{u}$ to the near-surface, compared to that found after an SSW onset (see figure 2 in the main article), is likely due to the inclusion of all negative NAM events in the stratosphere (no matter their magnitude) in the analysis here.

References

Andrews, D. G., J. R. Holton, and C. B. Leovy, 1987: *Middle Atmosphere Dynamics*. Academic Press, 489 pp.

Garfinkel, C. I., I. P. White, E. P. Gerber, M. Jucker, and M. Erez, 2019: The building blocks of northern hemisphere wintertime stationary waves. *J. Clim.*, **Submitted**.

Jucker, M., and E. P. Gerber, 2017: Untangling the annual cycle of the tropical tropopause layer with an idealized moist model. *J. Clim.*, **30**, 7339–7358.

Martineau, P., S.-W. Son, M. Taguchi, and A. H. Butler, 2018: A comparison of the momentum budget in reanalysis datasets during sudden stratospheric warming events. *Atmos. Chem. and Phys.*, **18 (10)**, 7169–7187, doi:10.5194/acp-18-7169-2018, URL https://www.atmos-chem-phys.net/18/7169/2018/.

Simpson, I. R., B. M., and J. D. Haigh, 2009: The role of eddies in driving the tropospheric response to stratospheric heating perturbations. *J. Atmos. Sci.*, **66**, 1347–1365.

LIST OF FIGURES

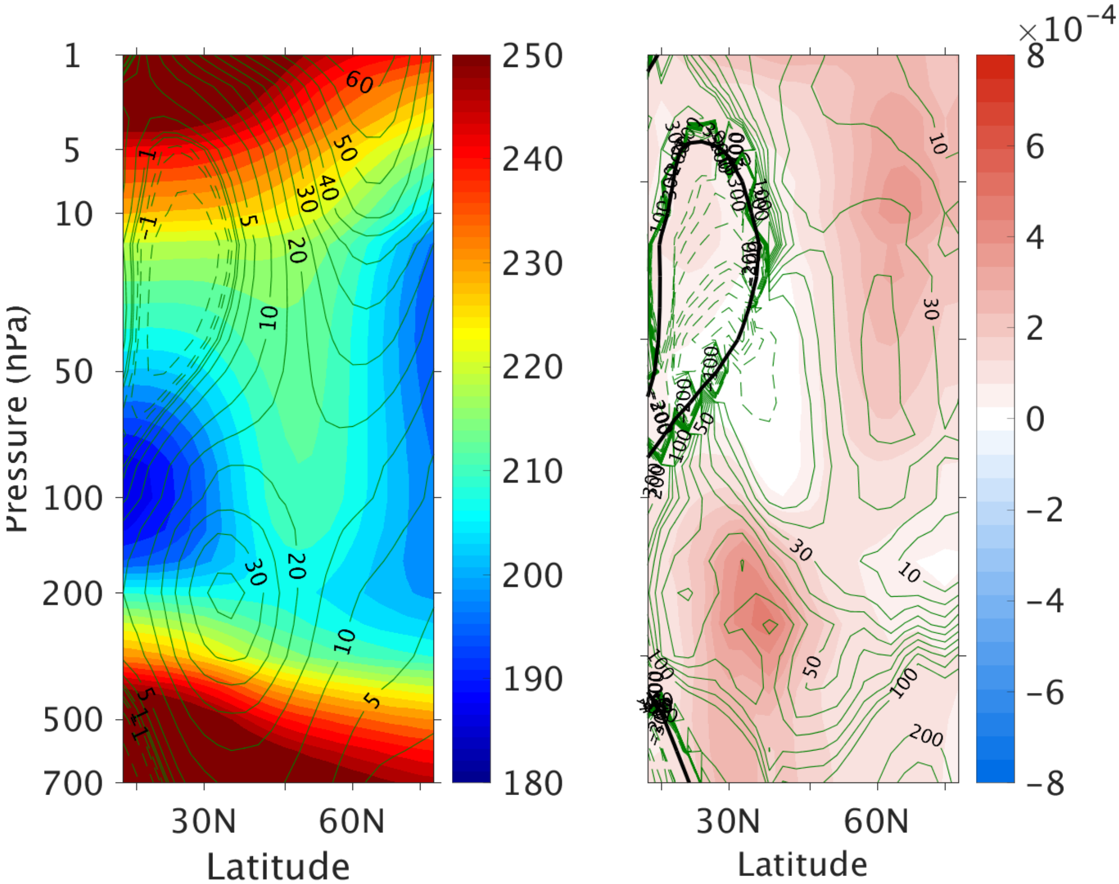

FIG. 1. (a) December-February climatologies of the zonal-mean zonal wind $\overline{u}$ (contours; units of m s^{-1}) and temperature $\overline{T}$ (shading; units of K) for CTRL. The contour spacing for $\overline{u}$ is $\pm$1, 2.5, 5, 10, 15,... m s^{-1}. (b) Same as (a) except for the quasi-geostrophic potential vorticity gradient $\overline{q}_{\varphi}$ (shading; units of s^{-1}) and refractive index n^2 (contours; dimensionless as scaled by a^2). n^2 has contours at values of $\pm$10,20,...,100,200,300,... . Thick black line is the December to February climatological zero-wind line.

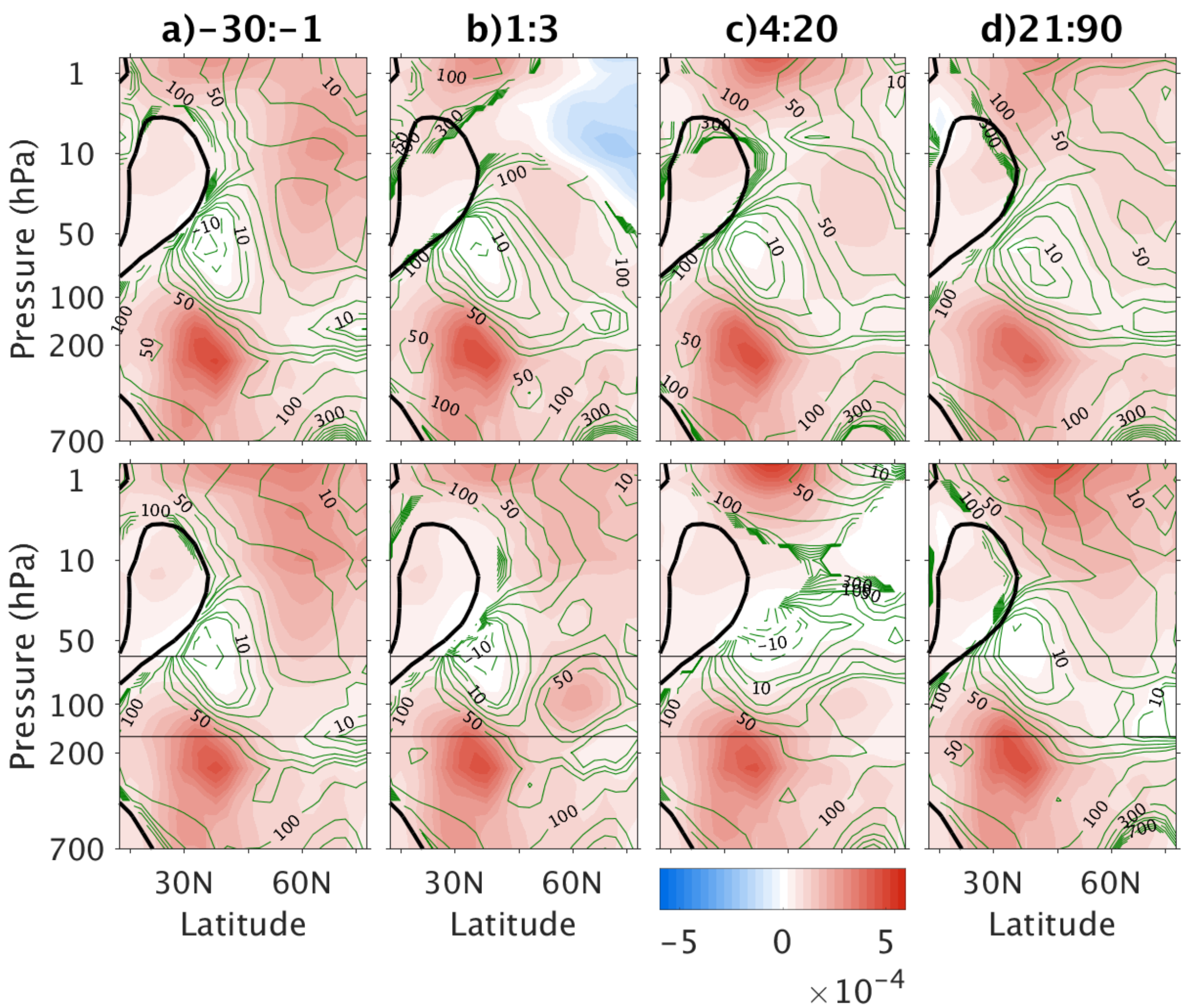

FIG. 2. Quasi-geostrophic refractive index (n^2; contours) and potential vorticity gradient ($\overline{q}_{\varphi}$; shading) averaged over various lag stages for CTRL (top) and the 15-K PTRB experiment (bottom). Solid (dashed) green contours indicate positive (negative) n^2. Note that the full field is presented here, in contrast the the anomalies in the main text. Further, n^2 has been scaled by a^2 and is hence dimensionless, whereas $\overline{q}_{\varphi}$ has units of s^{-1}. Contours of n^2 have been omitted where $\overline{u} < 0$ (N.B. that $\overline{u}$ is the full field and not the anomaly). See main text for details regarding the calculations for both CTRL and PTRB. Thick black line as in figure 1. Horizontal lines in the bottom row are as in figure 1b in the main text.

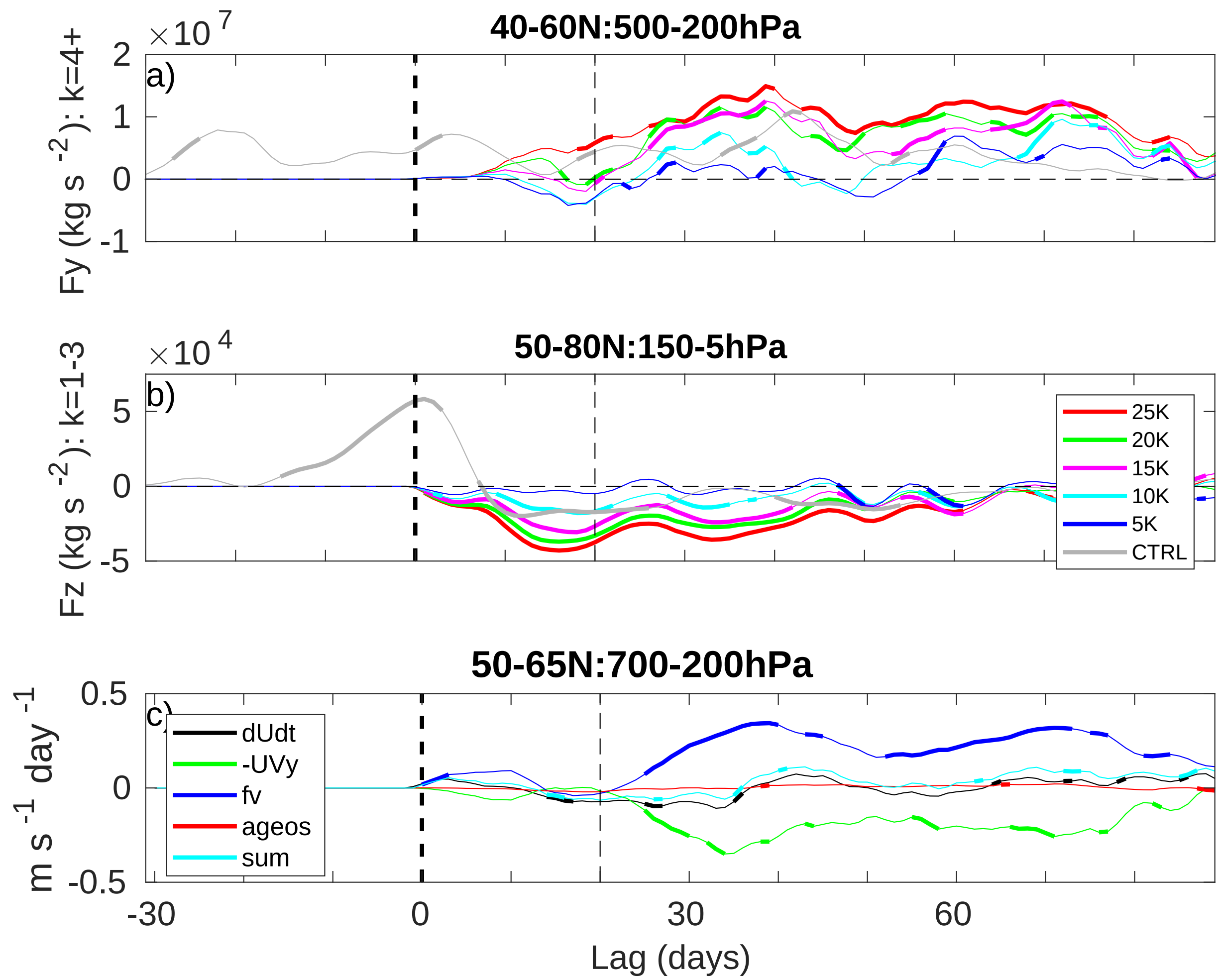

FIG. 3. Timeseries of (a) synoptic-wave $F^{(\varphi)}$ area-averaged over 40-60N and vertically integrated over 500 to 200 hPa, and (b) planetary-wave $F^{(z)}$ averaged over 50-80N and 150-5 hPa, for the ensemble means of each PTRB run and CTRL. Double-thickness lines indicate statistically-significant differences from the CTRL climatology at the 95% level. Note that (a) has been smoothed by a 9-day running mean to emphasise the salient features. (c) Timeseries of terms in the Eulerian mean momentum budget (eq. 1) for the 15-K PTRB as contributions to the acceleration of the zonal-mean zonal wind ($\partial\overline{u}/\partial t$). In the legend, dUdt represents $\partial\overline{u}/\partial t$, fv is the Coriolis torque acting on the mean meridional wind ($f\overline{v}$), $-$UVy is the eddy momentum flux convergence ($-(a\cos^2\varphi)^{-1}(\overline{u'v'}\cos^2\varphi)_\varphi$) and ageos represents the ageostrophic terms defined as $-\overline{v}(a\cos\varphi)^{-1}(\overline{u}\cos\varphi)_\varphi - \overline{w}\overline{u}_z - \rho_0^{-1}(\rho_0\overline{w'u'})_z$. The sum is calculated as the sum of all of the terms excluding $\partial\overline{u}/\partial t$. Note that the sum is approximately equal to $\partial\overline{u}/\partial t$ indicating that the budget nearly closes. Thick lines are the same as in a-b.

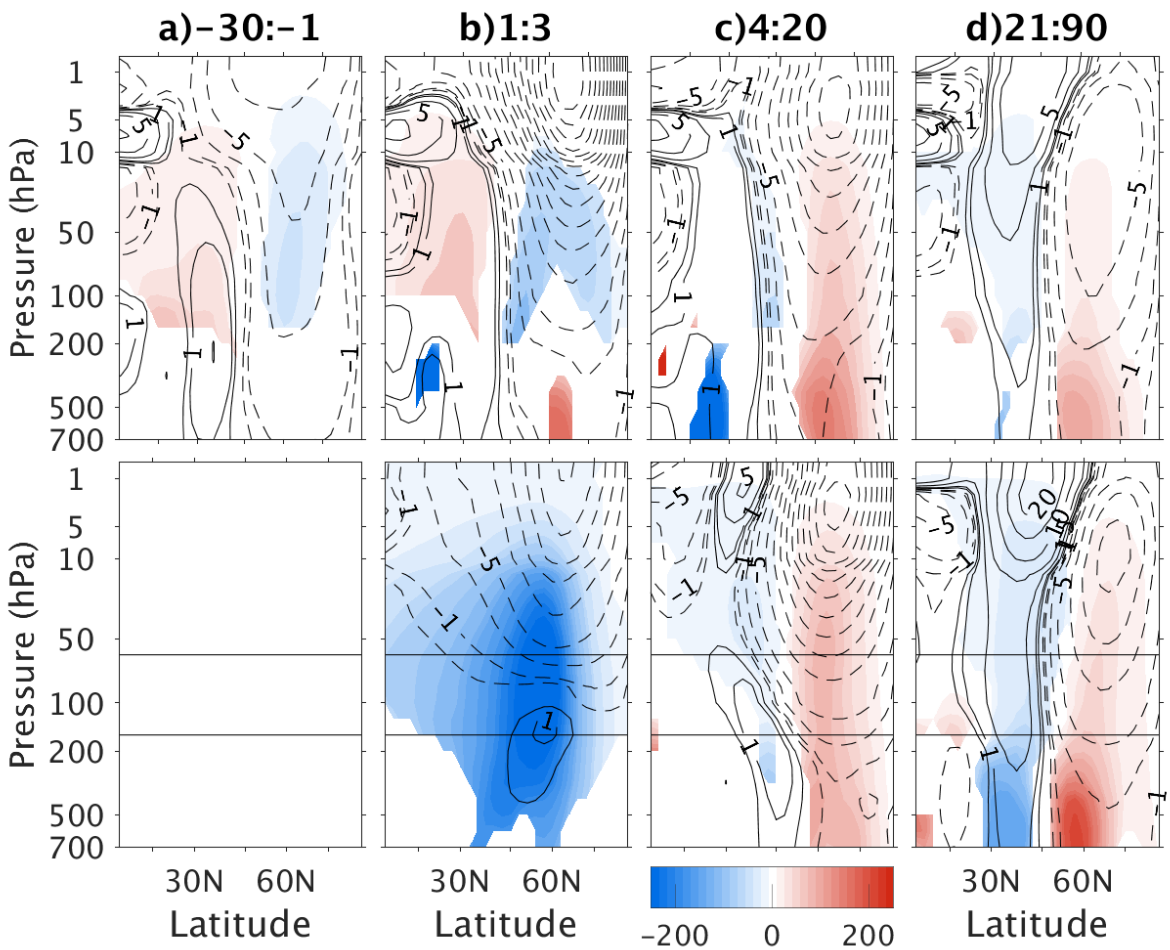

FIG. 4. As in figure 10 in the main manuscript except for latitude-height cross-sections of the contribution of $\Psi_{\overline{v}}$ (units of kg m s^{-2}) to Ψ^*, averaged over lags (a) -30–1, (b) 1-3, (c) 4-20, and (d) 21-90 for the CTRL (top row) and 15-K PTRB experiment (bottom row). Note that the two lag stages 4-10 and 11-20 in figure **??** have been averaged into a single panel here, for brevity. Note that only $\Psi_{\overline{v}}$ anomalies which are statistically significantly different from the climatology in CTRL are shaded. Black contours represent the corresponding $\overline{u}$ anomalies at these lags with contours at $\pm 0.5, 1, 2.5, 5, 10, \ldots$m s^{-1}.

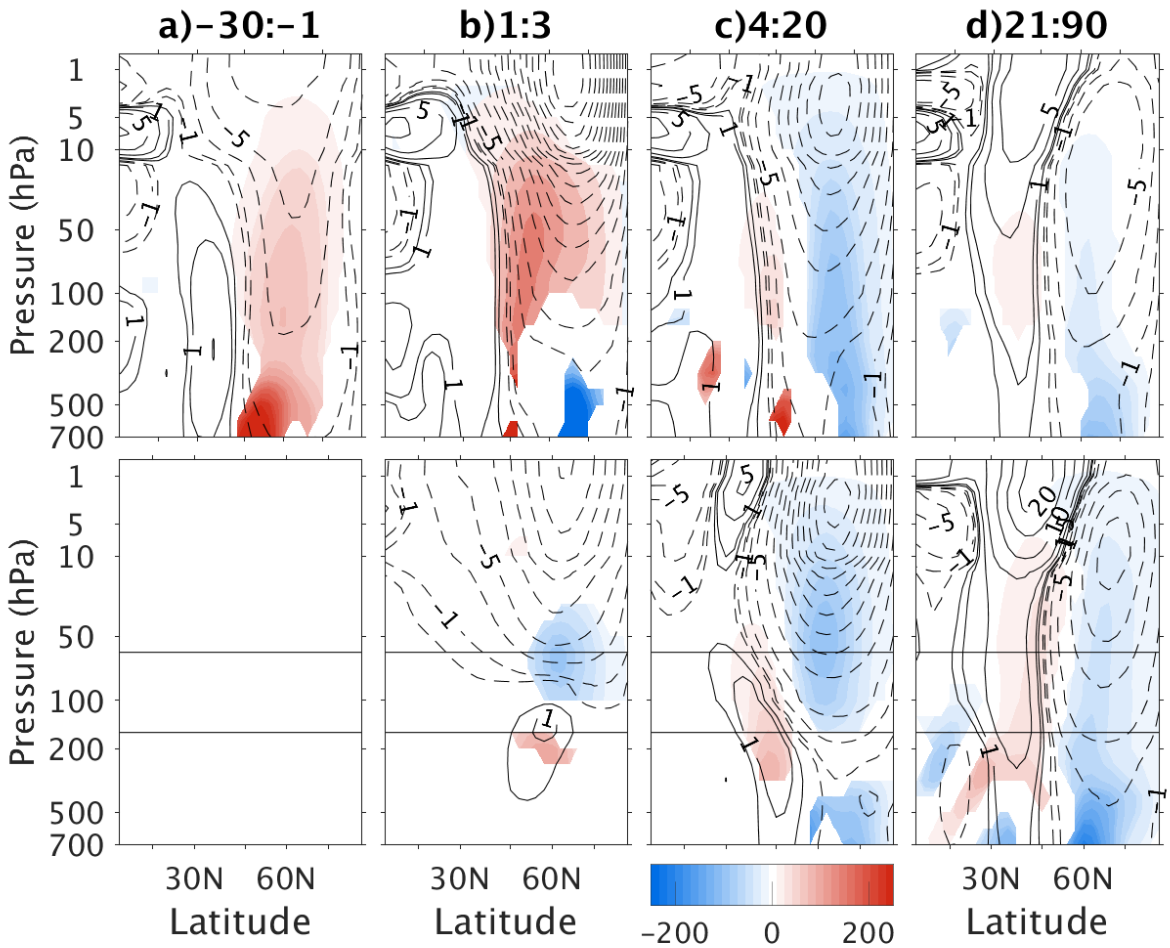

FIG. 5. Same as supplementary figure 4 except for $\Psi_{\overline{v'T'}}$.

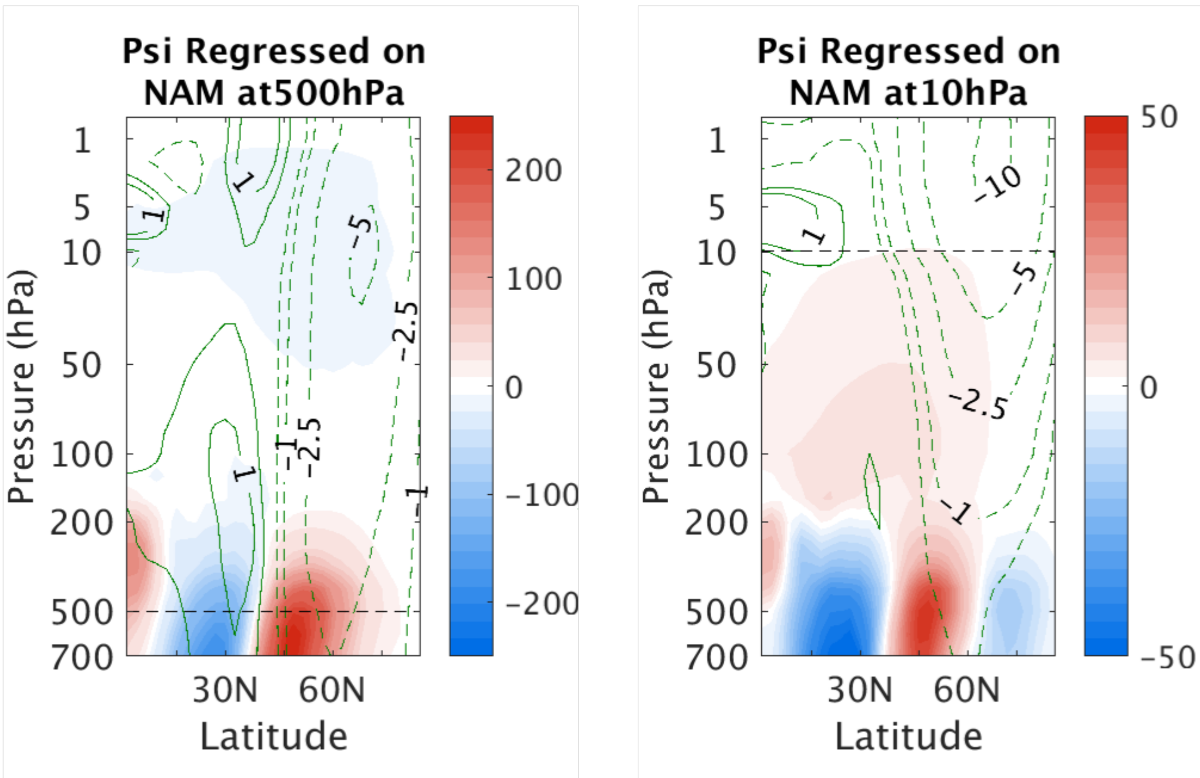

FIG. 6. The residual mean meridional circulation Ψ^* (shading; units of kg m s^{-2}) and $\overline{u}$ (green contours; units of m s^{-1}) regressed as a function of latitude and height onto the NAM index at (a) 500 hPa, and (b) 10 hPa. Note that the NAM index is calculated by projecting the daily area-weighted geopotential height anomalies (i.e., deviations away from CTRL climatology) onto the first empirical orthogonal function and then normalising by the standard deviation. The NAM index used here is highly correlated with that presented in the main text (figure 3). Horizontal black lines show the level which Ψ^* and $\overline{u}$ are regressed onto in each panel. Note the different colorbars for each panel.